Preliminary estimates of tritium permeation and retention in the first wall of DEMO due to ion bombardment

Nuclear Materials and Energy 28 (2021) 101039

Contents lists available at ScienceDirect

Nuclear Materials and Energy

journal homepage: www.elsevier.com/locate/nme

Preliminary estimates of tritium permeation and retention in the first wall of DEMO due to ion bombardment

R. Arredondo [a], K. Schmid [a], F. Subba [b], G.A. Spagnuolo [c]

[a] Max-Planck-Institut für Plasmaphysik, Boltzmannstr. 2, D-85748 Garching, Germany
[b] NEMO Group, Dipartimento ENERGIA, Politecnico di Torino, Torino, Italy
[c] EUROfusion Consortium, Programme Management Unit, Garching, Germany

ARTICLE INFO

Keywords:
DEMO
First wall
Permeation
Retention
TMAP
TESSIM

ABSTRACT

Tritium self-sufficiency presents a critical engineering challenge for DEMO, requiring efficient breeding and extraction systems, as well as minimizing tritium losses to the surrounding systems, such as plasma-facing components, vacuum vessel, cooling system, etc. Structural and plasma-facing components will act as a tritium sink, as tritium will be accumulated in the bulk of these components due to energetic particle bombardment and may permeate out of the vacuum system. The design of the plasma-facing components will consequently directly influence the plant lifetime, operational safety and cost of any future power plant. Therefore, modeling of tritium retention and permeation in these components is required for the engineering designs of the tritium breeding and safety systems. In this work, the diffusion-transport code TESSIM-X is benchmarked against the well-established TMAP7 code and a comparison with a simplified DEMO-relevant test case is performed. The use of either code for modeling of DEMO conditions is discussed. Following this, TESSIM-X is used to provide a preliminary assessment of tritium permeation and retention in the DEMO first wall, based on the current WCLL (Water Cooled Lithium Lead) and HCPB (Helium Cooled Pebble Bed) breeding blanket designs.

1. Introduction

A key design requirement for the future demonstration power plant DEMO will be tritium (T) self-sufficiency, i.e. the production of enough tritium during operation to offset tritium burn in the fusion reaction, as well as tritium losses. Additional T must also be bred to provide an initial start-up T inventory for future fusion reactors and to act as a safety margin in the event of unforeseen T losses during maintenance or off-normal events [1].

Therefore, the study of possible T losses is critical for the design of DEMO [2]. While T losses from the breeding blanket (BB) into the coolant are an active field of research, e.g. [3–5], T losses from the plasma side into the First Wall (FW) coolant have not been studied in as much detail, and are required for future design activities related to the DEMO breeding blanket and fuel cycle.

This work presents preliminary estimates of T retention and permeation in the DEMO BB FW due to T ion or charge-exchange neutral bombardment and T gas, based on simulations performed with the diffusion-transport code TESSIM-X [6–8]. For this purpose, the code has been benchmarked with the TMAP7 code [9] using a suitable DEMO-relevant optimized comparison scenario (Section 2). In Section 3, the modeling assumptions and simulation cases for DEMO are discussed, and the main results are listed in Table 3. The potential effects of a recombination-limited surface boundary regime is discussed in Section 4. The possible impact of T retention in the DEMO first wall on the fuel cycle is briefly discussed in Section 5, while Section 6 constitutes a summary of the main results and limitations of this work.

2. TMAP7 and TESSIM-X code comparison

The Tritium Migration Analysis Program version 7 (TMAP7) [9] has been widely used in the past for modeling of T diffusion, reaction and trapping, e.g. [10,11]. TMAP7 is capable of simulating diffusion of up to 10 species though arbitrary volumes and enclosures, separated by e.g. solution- or rate-dependent boundary conditions. One key feature of TMAP7 over its predecessor, TMAP4, is the ability to compute up to 3 traps for diffusion through solid structures.

TESSIM-X [6,8] is a diffusion-trapping code capable of modeling hydrogen isotope diffusion through multiple solid enclosures, with an arbitrary number of trap energies and profiles, as well as modeling of

E-mail address: rodrigo.arredondo@ipp.mpg.de (R. Arredondo).

https://doi.org/10.1016/j.nme.2021.101039
Received 1 April 2021; Received in revised form 18 June 2021; Accepted 5 July 2021
Available online 8 July 2021

fill-level dependent trapping [7].

Two main concepts are considered for the DEMO breeding blanket first wall. These are the Water-Cooled Lithium Lead [12] (WCLL) and Helium-Cooled Pebble Bed [13] (HCPB) concepts. They differ in the type of coolant (water at 155 bar and temperature between 295 and 328 °C or helium at 80 bar and temperatures between 300 and 520 °C, respectively) as well as for the kind of breeder (eutectic alloy of PbLi or orthosilicate), neutron multiplier (e.g. Pb or beryllide, respectively) and T-carrier (e.g. PbLi itself or He purge-gas, respectively). From the point of view of the plasma-facing first wall, both concepts envision a 2 mm W-containing cladding, followed by a EUROFER structure fitted with cooling channels. However, the difference in cooling medium (water and helium, respectively) leads to a difference in temperature profiles, with the HCPB concept expecting W surface temperatures roughly 120 °C higher than those for the WCLL concept. As a consequence of these higher temperatures, the EUROFER wall thickness is also smaller in the HCPB concept (2 mm vs. 3 mm for the WCLL concept).

A code comparison was performed utilizing the TMAP7 and TESSIM-X codes for both the WCLL and HCPB first wall temperature profiles and geometries. The W cladding was assumed to behave as pure W, with solubility and diffusion data taken from [14], while the data from [15] were used for EUROFER. It should be noted that a discrepancy is present in the physical properties of EUROFER as listed in [15]: While the solubility pre-factor $K_{s,l0}$ is listed as 1.02×10^{-3} mol m^{-3} Pa$^{-1/2}$, dividing the permeability by the diffusivity yields a pre-factor of 1.02×10^{-1} mol m^{-3} Pa$^{-1/2}$. In this work, the latter value is assumed, as it is the one listed in [16] and shows better agreement with other values in the literature [17]. Based on [12,13], a temperature gradient of 673 K to 663 K for W and 663 K to 613 K for EUROFER was assumed for the WCLL scenario, whereas for the HCPB scenario temperature gradients of 793 K to 783 K for W and 783 K to 683 K for EUROFER were assumed.

Dirichlet boundary conditions were employed at the inlet and outlet sides by applying Sieverts' law thus assuming equilibrium with the ambient gas pressure. A T partial pressure of 1 Pa was assumed on the plasma side, while on the coolant side the T partial pressure was set to 0 Pa which is equivalent to a diffusion limited boundary. Continuity at the W/EUROFER interface was maintained by applying mass conservation (equal diffusion fluxes) and equilibrium of the chemical potentials on each side of the material interface.

The chemical potential of H isotopes in a metal X with heat of solution E^X_{SOL}, non configurational entropy ΔS^X and number of tetrahedral sites per atom γ as function of Temperature T is calculated is in eq. (1).

$$\mu_{HinMat.X}\left(C^X_{SOL}, E^X_{SOL}\right) = E^X_{SOL} - T\Delta S^X - K_B T ln\left(\frac{\gamma}{C^X_{SOL}}\right) \quad (1)$$

To determine the parameters in eq. (1), the chemical potential in the metal is set to be equal to the chemical potential of the ideal gas and this equation is then solved for C^X_{SOL} yielding eq. (2).

$$C^X_{SOL} = \gamma e^{\frac{\Delta S^X}{K_B}} \sqrt{\frac{P}{P_0}} e^{\frac{-E^X_{SOL}}{K_B T}} \quad (2)$$

Comparing this result with Sieverts' law $C^X_{SOL} = K_{s,l0} e^{\frac{-E^X_{SOL}}{K_B T}}$ allows to obtain ΔS^X and E^X_{SOL}. This procedure yields the paramteres in Table 1 for W [14] and EUROFER [15] for given values of $\gamma = 8$ for both W and EUROFER.

Table 1
Chemical potential parameters for W [14] and EUROFER [15] used in this work.

Parameter	Value
E^W_{SOL}	1.14 eV
$E^{EUROFER}_{SOL}$	0.238 eV
$e^{\frac{\Delta S^W}{K_B}}$	3.42×10^{-3}
$e^{\frac{\Delta S^{EUROFER}}{K_B}}$	1.53×10^{-6}

The influx of T due to energetic particle bombardment was modeled as a source term with a Gaussian profile. The mean implantation depth and standard deviation were taken as 3.8 nm and 2 nm, respectively, based on static SDTrimSP [18,19] simulations of 100 eV T bombardment on W. The impinging flux was set to 8×10^{19} T m^{-2}s^{-1}, but due to the reflection coefficient of 0.64 from the SDTrimSP simulations, it was reduced to 2.88×10^{19} T m^{-2}s^{-1}. The impinging particle fluxes and energies are within the assumed ranges given in [20].

While trap concentrations and energies do not affect the steady-state permeation flux, they do impact the onset of permeation and transient permeation behavior, as well as the total retained amount of T. One trap energy was included in the model system for each layer. For W, this energy was 1.4 eV, while for EUROFER it was 0.6 eV. The trap concentration was in all cases 5×10^{-5} for each trap type. These values are consistent with literature data for trap site concentrations in the bulk of unirradiated W and EUROFER, e.g. [15,21].

Fig. 1 shows the T permeation flux density (a) and retained T amount (b) as a function of time (in full-power days) for the WCLL (blue) and HCPB (red) scenarios modeled with TMAP (dashed lines) and TESSIM (solid lines). A second ordinate axis is included in these two plots, assuming a first wall surface area of 1400 m^2 [22]. The solute (c) and trapped (d) T concentration profiles are also shown at the final time step. For the WCLL scenario, this time was 10 million seconds (roughly 120 full-power days). In the case of the HCPB scenario, as steady-state behavior is reached much sooner, the total simulated time was 5 million seconds (60 full-power days). The different exponents at the top of the ordinate axis should be noted, particularly when comparing (c) and (d), which show that trapping in W drives retention, while retention in EUROFER and the retained amounts in the solute are negligible. As a consequence of the lower temperatures, more traps are filled with T in the WCLL scenario than in the HCPB scenario. This also has the effect of delaying the onset of permeation and the point when the steady-state permeation flux is reached in the WCLL case relative to the HCPB case.

As is seen in Fig. 1, there is good agreement between TMAP7 and TESSIM-X in all cases. However, as mentioned above, the trap energies and concentrations employed in the code comparison reflect values in unirradiated materials. When taking into account neutron irradiation, higher trap energies and trap concentrations are expected [23,24]. Trap concentrations in W may be increased further in the event of simultaneous hydrogen isotope loading during damaging, as may be the case for DEMO, reaching the sub-% range [24]. When modeling these increased trap concentrations with TMAP7, severe computational performance issues arise. For instance, one WCLL simulation with trap concentrations of 0.1% may take over 100 days to complete, while it may be accomplished with TESSIM-X within 2–4 h. In addition to drawbacks in performance, limitations in the TMAP7 code hamper its use for modeling of irradiated W. In [24], irradiated W is modeled with a total of 5 trap energies, ranging from 1.35 eV to 2.1 eV. These trap energies cannot be implemented in TMAP7, as the code can compute a maximum of 3 trap types. Given these issues with TMAP7, and that good agreement between TMAP7 and TESSIM-X has been shown for the DEMO-relevant optimized scenario, the following assessments of T permeation and retention in the DEMO first wall are all performed with TESSIM-X. Where feasible, TMAP7 simulations have also been performed, maintaining good agreement with the TESSIM-X simulations, but have been omitted from the following figures in the interest of clarity.

3. T permeation and retention in the DEMO first wall

The following DEMO assessments pertain exclusively to the first wall, and do not account for possible permeation nor retention in the divertor or baffle regions. The previously used WCLL and HCPB geometries, thermal profiles, boundary conditions, solubilities and diffusivities were maintained. However, the impinging particle fluxes and

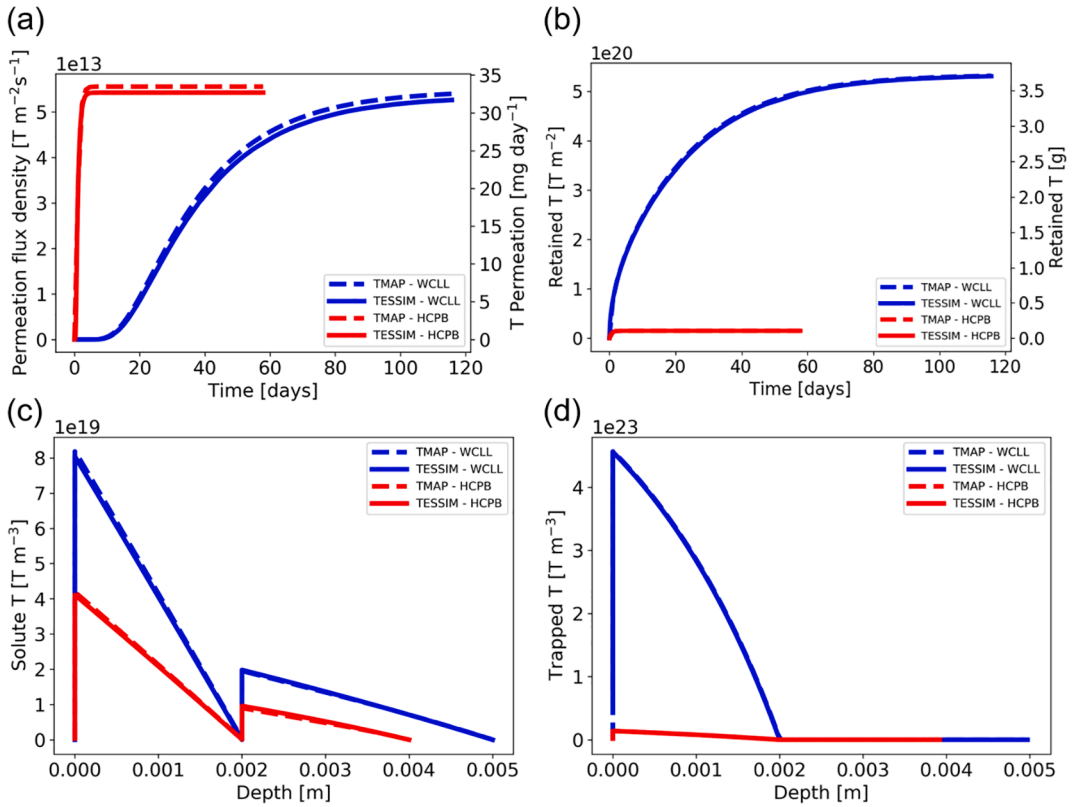

Fig. 1. (a) T Permeation flux density and (b) total retained T as a function of time, in full-power days, for the WCLL and HCPB scenarios modeled with TMAP7 and TESSIM-X. An additional ordinate axis assuming a 1400 m^2 first wall is included for clarity. The solute (c) and trapped (d) T concentration profiles are plotted at the last time-step of 5 $\times$ 10^6 s for the HCPB scenario and 10^7 s for the WCLL scenario, i.e. roughly 60 full-power days and 120 full-power days, respectively. The exponents at the top of the ordinate should be noted.

energies, as well as the trap concentrations and energies, were modified to more closely model the conditions expected for DEMO, as is discussed in more detail below.

The impinging particle fluxes and energies used for the DEMO assessments were based on SOLPS-ITER simulations [25] of deuterium plasmas with the current DEMO geometry, which includes limiters. The impinging T particle energy was set to 500 eV, resulting in an average implanted depth in W of 9.8 nm with an ion range straggle of 5.4 nm and a reflection yield of 0.56, based on static calculations with SDTrimSP [18,19]. Large variations in the impinging particle fluxes are present in the SOLPS-ITER simulations, depending on e.g. assumptions in the plasma fueling model. To account for these variations, all simulations were performed with impinging T particle flux densities of 10^{18}, 10^{19} and 10^{20} T m^{-2}s^{-1}.

As previously stated, all simulations were performed for T. However DEMO will operate with a mixture of deuterium and tritium. If the impinging flux is assumed to consist of 50% D and 50% T, and the slight differences in e.g. reflection and implantation depth are ignored, then it can be assumed that the steady state T permeation rate and T retention would also be 50% of the values obtained from the simulations with only T.

As shown in [24], trap concentrations in W are a function of temperature and increase with the level of damaging, with higher trap concentrations being reached in the event of simultaneous hydrogen isotope loading. There is evidence that, in the temperature range between 600 K and 800 K, at a damage level of 0.35 dpa (displacements per atom), saturation is reached [23,24]. Based on this data, it was decided to investigate four distinct damaging scenarios: the "no dpa" scenario features low trap concentrations and no high-energy traps are present (2.1 eV for W, 1.35 eV for EUROFER). The "low dpa" scenario aims to reproduce trap concentrations at 1/10th of the saturation dpa, i.e. 0.035 dpa. The remaining two scenarios, "high dpa" and "high dpa + high D/T" represent trap concentrations at the saturation damaging value of 0.35 dpa, with and without the effect of damage stabilization [24] by simultaneous hydrogen isotope loading.

Table 2 lists the trap concentrations for W for the four investigated damaging scenarios at the WCLL and HCPB relevant temperatures, as obtained from [24]. The trap concentrations listed for defect type 1 are

Table 2
Trap concentrations in W assumed for the four investigated damaging scenarios and FW concept, based on [24]. Defect 1 corresponds to detrapping energies of 1.35 eV and 1.46 eV, defect 2 to 1.68 eV and 1.86 eV, while defect 3 corresponds to a detrapping energy of 2.1 eV. The right-most column represents the estimated time required to reach the corresponding damaging regime, in full-power days [22].

DPA		Wall concept	Defect 1 [%]	Defect 2 [%]	Defect 3 [%]	Time [days]
No dpa		WCLL	0.01	0	0	0
		HCPB	0.01	0	0	
0.035		WCLL	0.1	0.1	0.025	3
		HCPB	0.05	0.07	0.025	
0.35	Low D/T	WCLL	0.14	0.14	0.05	26
		HCPB	0.07	0.1	0.05	
	High D/T	WCLL	0.4	0.2	0.05	
		HCPB	0.1	0.1	0.05	

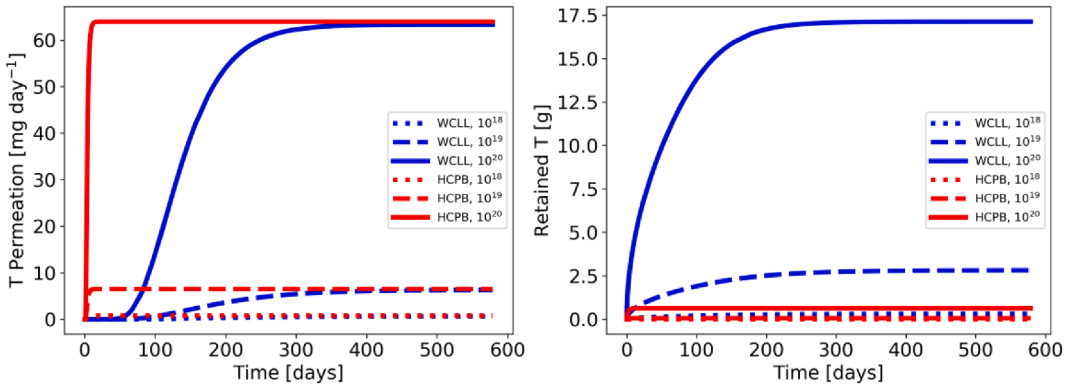

Fig. 2. T permeation rate, in full-power days, and total retained T as a function of time, also in full-power days, under the "no dpa" damaging scenario for the WCLL (blue) and HCPB (red) concepts. Dotted lines indicate an impinging particle flux of 10^{18} T m^{-2}s^{-1}. Dashed lines correspond to a flux of 10^{19} T m^{-2}s^{-1}, and solid lines indicate a flux of 10^{20} T m^{-2}s^{-1}. The results are scaled assuming half of the impinging particle flux is T and half is D. (For interpretation of the references to color in this figure legend, the reader is referred to the web version of this article.)

divided equally among two single occupancy traps with detrapping energies of 1.35 eV and 1.46 eV. Defect type 2 also corresponds to two traps with detrapping energies of 1.68 eV and 1.86 eV, while the defect type 3 traps correspond to a single detrapping energy of 2.1 eV. The right-most column represents the estimated maximum time in full-power days required to reach the corresponding damage level in W, assuming a damage rate of 5 dpa/fpy (full-power year) [22]

For EUROFER, two trap energies of 0.65 eV and 1.35 eV are included in the model, based on data from [23,26,27]. The trap concentrations were varied between 5×10^{-5} and 2×10^{-3}, following the same scaling as for W. While there is no conclusive evidence of increased trap concentrations due to simultaneous hydrogen isotope loading for EUROFER, this was assumed in the "high dpa + high D/T" case as a conservative estimate. Nevertheless, due to the lower detrapping energies, the overall effect of the EUROFER traps is negligible relative to that of the W traps.

Fig. 2 shows the T permeation rate in full-power days and total retained T amount in the WCLL (blue) and HCPB (red) DEMO FW as a function of time, also in full-power days, for the "no dpa" scenario, assuming an impinging T content of 50%. Simulations performed with impinging particle fluences of 10^{18}, 10^{19} and 10^{20} T m^{-2}s^{-1} are plotted with dotted, dashed and solid lines, respectively. Due to the larger trap energies and concentrations in this scenario than in the simplified model shown in Fig. 1, the onset of permeation is delayed and the amount of retained T is increased in this scenario relative to the simplified model system discussed in Section 2.

Under these conditions permeation is foreseen in all cases in DEMO within the first 600 days. As ion driven permeation in a diffusion-limited regime is temperature independent [28], the expected steady state permeation flux is the same for the WCLL and HCPB concepts (the difference in the EUROFER thickness is negligible). Due to the lower temperature, retention is larger for the WCLL concept than for the HCPB concept for the same impinging flux. This value lies just under 17.5 g for the highest flux assumption at the end of the simulated time for WCLL, while for HCPB it is roughly 0.5 g. However, as was listed in Table 2, the "no dpa" scenario should only be valid for, at most, 3 full-power days. Thus, no permeation should be foreseen for the "no dpa" scenario within the time-frame where this scenario is valid.

If a higher damage level is assumed, the onset of permeation is delayed for all scenarios beyond the simulated 600 full-power days. The higher trap concentrations also lead to a significant increase in retention, as is shown in Fig. 3 for the 0.035 dpa (i.e., "low dpa") and 0.35 dpa ("high dpa") with simultaneous hydrogen isotope loading scenarios. In this last scenario, T retention after 600 full-power days can reach 350 g for the WCLL concept and 200 g for the HCPB concept. For reference, the in-vessel T inventory limit for ITER is set to 1 kg [10], while the values considered for safety assessments for DEMO may be substantially higher [29].

Up to now, both FW concepts have been modelled assuming that the 2 mm W-containing cladding has the properties of pure W. However, to reduce thermal stresses, the current reference design for this cladding consists of a 0.8 mm pure W layer followed by a series of W/EUROFER functionally-graded material (FGM) interlayers with a total thickness of

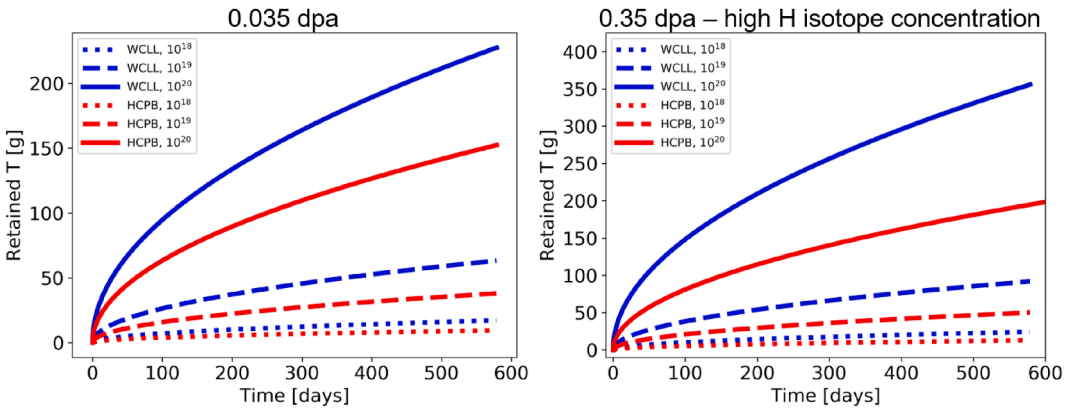

Fig. 3. T retention as a function of time under the "low dpa" and "high dpa + high D/T" damaging scenarios, for the WCLL (blue) and HCPB (red) concepts. The line style codifies the assumed impinging particle flux with a T content of 50%. (For interpretation of the references to color in this figure legend, the reader is referred to the web version of this article.)

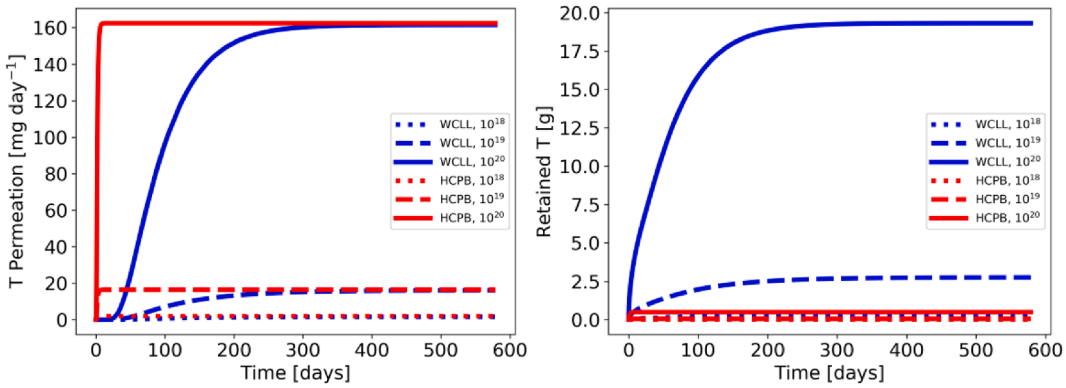

Fig. 4. T permeation rate and retention for the WCLL (blue) and HCPB (red) concepts under the "no dpa" scenario as a function of time, assuming a 0.8 mm W cladding, and the remaining 1.2 mm of W-containing FGM layers behaving like EUROFER. Time is plotted in full-power days. The line style indicates the impinging particle flux density, assuming 50% is T. (For interpretation of the references to color in this figure legend, the reader is referred to the web version of this article.)

1.2 mm [30–32]. Sound modeling of these FGM layers is currently infeasible, as key data such as their hydrogen diffusivity and solubility, trap concentrations and interface properties are currently unknown. Therefore, an alternative to modeling the FGM layers as W would be to model them with the properties of EUROFER, thereby hoping to provide upper and lower bounds to the actual permeation and retention behavior for DEMO. Indeed, this alternative approach could prove to be the more realistic assumption. Given the lower enthalpy of solution of hydrogen in EUROFER [15] compared with that of hydrogen in W [14], it would be reasonable to assume that hydrogen isotopes in W would preferentially enter the EUROFER phase, and that diffusion through EUROFER grains would provide the most favorable pathway for permeation. The temperature gradient for the WCLL scenario was set to 673 K to 669 K for W and 669 K to 613 K for EUROFER. For the HCPB scenario, these gradients were 793 K to 789 K for W and 789 K to 683 K for EUROFER. Fig. 4 is the analogue of Fig. 2, showing the T permeation and retention behavior in the "no dpa" scenario, assuming a 0.8 mm pure W cladding and modeling the 1.2 mm of FGM layers like EUROFER. Due to the smaller thickness of the W layer, permeation is increased significantly. Retention, on the other hand, is roughly the same, as the trap concentrations in the W and EUROFER are comparable in the "no dpa" scenario. The slight increase in retention in the highest flux WCLL case is attributed to the slightly different temperature gradient in the EUROFER layer, which was necessary to ensure the same temperatures at the W and EUROFER surfaces.

Despite the reduced breakthrough time when assuming this new wall geometry, permeation still does not occur within the first 3 full-power days of operation, when the "no dpa" scenario is valid. In the "low dpa" scenario, the onset of permeation is further delayed, beyond the time-window where the "low dpa" scenario is valid. Fig. 5 shows T retention under the 0.35 dpa ("high dpa") damage scenarios, with (right) and without (left) H isotope loading, when assuming a 0.8 mm pure W cladding. In order to study the long-term trend of retention, these simulations were performed up to time scales larger than 10 fpy. This is in excess of the actual projected lifetimes of the DEMO breeding blankets, which are currently around 2 fpy for the 1st BB and 5 fpy for the 2nd BB [22]. These simulations show that, even with a reduced W cladding of 0.8 mm, permeation within the lifetime of the breeding blankets only happens under the highest flux assumptions. Permeation in the WCLL scenario only occurs if no increased trap concentrations due to simultaneous hydrogen isotope loading are assumed. In these time scales, T decay will play a significant role on the actual T inventory. However, T decay has not been implemented into the simulations. Therefore, the values for retention shown in Fig. 5 should be viewed at T losses, assuming the wall acts as a sink for T, and not as actual T inventories.

A third wall scenario was investigated for DEMO, consisting of a pure EUROFER wall. This could be the case either if the W-containing cladding were removed e.g. due to erosion, or if a bare EUROFER wall were installed as plasma-facing material in recessed areas of DEMO [33,34].

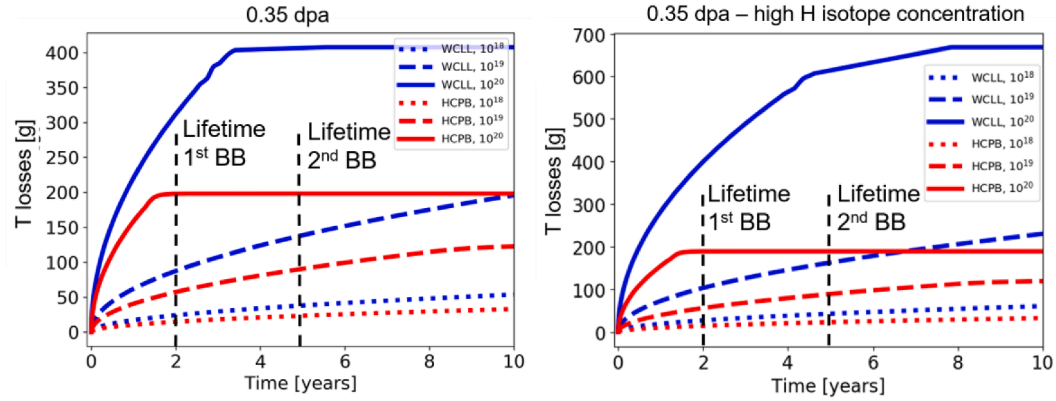

Fig. 5. T lost due to retention in the DEMO FW as a function of time, in full-power years, assuming a 0.8 mm W cladding. Damage scenarios of 0.35 dpa without hydrogen isotope loading (left) and with hydrogen isotope loading (right) were used. T decay is not considered in these simulations. The color and line style convention is the same as in the previous figures.

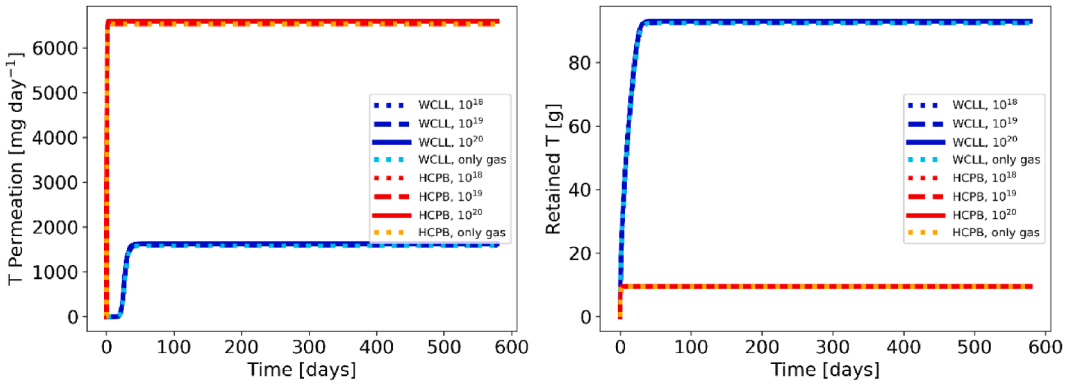

Fig. 6. T permeation and retention as a function of time (in full-power days) when assuming a EUROFER-only wall under the highest damaging scenario (0.35 dpa and simultaneous hydrogen isotope loading). The color and line style convention is the same as in the previous figures, with the addition of the cyan and orange dotted lines. These represent T permeation and retention with only T gas loading at a pressure of 1 Pa and no ion loading. (For interpretation of the references to color in this figure legend, the reader is referred to the web version of this article.)

For this scenario, the thickness of the pure EUROFER layer was maintained, and the 2 mm of W-containing cladding was removed, i.e., the wall thickness is 3 mm for the WCLL concept and 2 mm for the HCPB concept. Due to the fast T permeation through EUROFER at DEMO-relevant temperatures and the relatively low trap energies, in this scenario the onset of permeation is quickly reached regardless of damage level, but retention is quite modest compared to the W-containing scenarios. Fig. 6 shows the T permeation rate and T retention in the EUROFER-only case with the highest trap concentrations, i.e. the "high dpa" scenario with simultaneous hydrogen isotope loading. A T content of 50% in the impinging particle flux was assumed. Due to the higher solubility of T in EUROFER compared with that of T in W, with a bare EUROFER wall, gas-driven T loading dominates permeation and retention, as represented by cyan and orange dotted lines in Fig. 6 for the WCLL and HCPB concepts, respectively. Permeation is particularly large at the higher temperatures of the HCPB concept.

T permeation occurs almost immediately for the HCPB concept regardless of the impinging particle flux, while in the WCLL concept there is still a breakthrough time of roughly 25 full-power days. Retention in the HCPB concept is low (13 g), while in the WCLL concept it is higher (up to 93 g), but still modest compared with the W-containing scenarios.

As conservative (worst-case) estimates of T permeation and retention in DEMO, the values for the highest flux assumption (10^{20} D/T m^{-2}s^{-1}) for all investigated wall geometries and concepts are listed in Table 3 for the 0.35 dpa damaging scenarios, with and without simultaneous H isotope loading. The data is evaluated at the end of life of the 2nd BB (5 fpy) and assumes 50% of the impinging flux is T.

4. Implication of possible surface limits on permeation and retention

The diffusion trapping calculations presented above were performed by assuming an ideal surface, i.e. the release of T from the surface being only limited by diffusion to the surface. However experimental data on surface limited release for W exists and its implication on the above results needs to be discussed. A surface limit on the outlet side would decrease the permeation rate but would not affect retention since all traps are already filled once permeation breakthrough occurs regardless of whether or not a recombination limit is present. Therefore, the outlet side would not affect the upper limit estimates with regard to permeation and retention. However, a recombination limit on the inlet side could increase the subsurface solute concentration CS0 for plasma loading. For pure gas loading (dominant for the EUROFER-only scenarios) Sieverts' law sets the surface concentration which in steady state is not affected by a surface limit. Therefore, only for plasma loading an increase in CS0 would increase the gradient into the bulk and thus increase both the rate at which the traps are filled and the permeation flux once all traps are filled, i.e. after breakthrough of the permeation front. Thus, a permeation limit on the inlet side might lead to a larger trapped amount at times prior to breakthrough, a shorter time to breakthrough and to a larger permeation flux after breakthrough. Naturally, after breakthrough the trapped amounts are the same as without a surface limit.

The use of recombination rate coefficients has recently been reviewed in [35]. It was shown that for implantation sources from plasmas or ion beams the standard Waelbroeck-type recombination limit is insufficient to explain the possible limits at the surface. Using the more complete model by Pick & Sonnenberg [36], the measurement of the

Table 3
T permeation rate and T retention losses at the end of life of the 2nd BB for all investigated scenarios for a damage level of 0.35 dpa, with and without simultaneous H isotope loading, assuming the impinging particle flux of 10^{20} D/T m^{-2}s^{-1} is 50% T.

Wall geometries	Wall concept	H isotope concentration	Permeation [mg T day^{-1}]	Retention losses [g T]
2 mm W cladding	WCLL	Low	0	488
		High	0	615
	HCPB	Low	0	347
		High	0	347
0.8 mm W cladding	WCLL	Low	161	407
		High	0	615
	HCPB	Low	161	189
		High	161	189
EUROFER only	WCLL	Low	1625	30
		High	1625	93
	HCPB	Low	6593	5
		High	6593	13

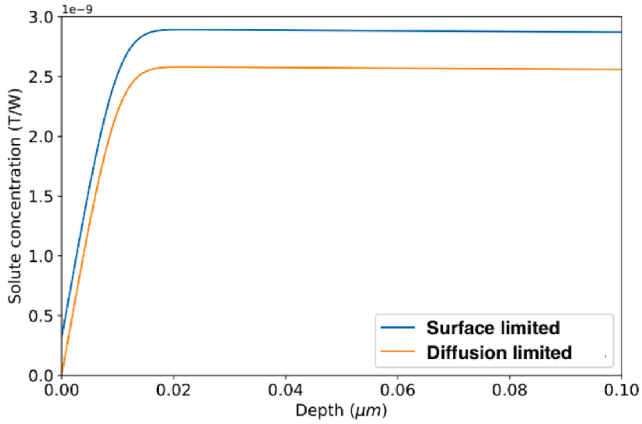

Fig. 7. Comparison of the solute depth profile for the HCPB case under the 0.35 dpa trapping scenario with an influx of 10^{20} m^{-2} s^{-1} with surface limited or diffusion limited boundary conditions.

recombination limit for W by Anderl [21] was investigated and appropriate surface parameters were extracted. Using these parameters in the implementation of the Pick & Sonnenberg model in TESSIM-X, the calculation for 0.8 mm W on EUROFER case for the HCPB concept under the 0.35 dpa trapping scenario was repeated at the highest plasma flux of 10^{20} T m^{-2} s^{-1}. This high flux case should be most affected by a surface limit. The calculation with surface limit resulted in an increase of the boundary concentration at the surface from 5×10^{-12} (solubility in W at 1 Pa and 793 K) to 3×10^{-10} T/W. However, as can be seen in Fig. 7, the gradient into depth is pivoted deeper in the sample approximately at the mean projected range of the ions. There the same increase occurs but the relative change is much smaller, from 2.6×10^{-9} to 2.9×10^{-9}, i.e. only an 11% increase. Since the gradient in depth is approximately directly proportional to this concentration, the same increase can also be expected for the permeating flux. Therefore a diffusion limited boundary condition may underestimate the permeation flux by ~ 10%. This can be considered within the uncertainties of the other input parameters.

5. Impact of retention on the T fuel cycle

Tritium sequestered in the first wall of DEMO may potentially constitute an issue for the T fuel cycle, as the temperatures required to desorb the retained T (>550 °C) are not easily achievable in DEMO without compromising the structural integrity of EUROFER [37]. Consequently, retained T might only be effectively desorbed at the end of life of the breeding blanket, which may prove problematic due to the activation of the BB segments and loss of T inventory through radioactive decay.

In [38], a simplified equation system is proposed to establish a particle balance model. This model is used to identify an upper limit for T loss probability in the plasma-facing components, i.e. the likelihood that a T atom reaching the wall is trapped. Implicit in the model is the assumption that all T pumped in the divertor region, extracted from the breeding modules or permeating into the coolant is recovered with perfect efficiency. Thus, the model only calculates the additional tritium required to compensate T burn and T lost due to trapping in the plasma-facing components. First, a particle balance is established:

$$\dot{M}_{inject} = \dot{M}_{burn} + (1 - R)\dot{M}_{wall} \tag{3}$$

where $\dot{M}_{inject}$, $\dot{M}_{burn}$ and $\dot{M}_{wall}$ represent the injected, burnt and wall mass flow rates of T, respectively, and R is the recycling coefficient, encompassing both reflected and thermally effusing T particles. The burnt T rate is defined as a fraction of the injected T:

$$\dot{M}_{burn} = p_{burn}\eta_{pellet}\dot{M}_{inject} \tag{4}$$

where p_{burn} represents the probability that a T nucleus in the plasma is burnt before escaping the plasma and η_{pellet} is the pellet fueling efficiency. The rate of T trapped in the wall ($\dot{M}_{trapped}$) is defined as the wall flow rate multiplied by a trapping probability ($p_{trapped}$):

$$\dot{M}_{trapped} = p_{trapped}\dot{M}_{wall} \tag{5}$$

The rate of excess T bred (tritium bred in excess of the burned amount) is defined as a function of the burn T rate and the tritium breeding ratio TBR:

$$\dot{M}_{bred} = (TBR - 1)\dot{M}_{burn} \tag{6}$$

Lastly, as condition for T self-sufficiency, the rate of excess T bred must be greater than the rate of trapped T, i.e.:

$$\dot{M}_{bred} \gg \dot{M}_{trapped} \tag{7}$$

By combining these simple equations, $p_{trapped}$ can be expressed by the following inequation:

$$p_{trapped} \ll (TBR - 1)(1 - R)\frac{p_{burn}\eta_{pellet}}{1 - p_{burn}\eta_{pellet}} \tag{8}$$

This result appears somewhat surprising, as it seems the upper limit for $p_{trapped}$ increases for decreasing$R$. The model as it is presented in [38] does not include the possibility of recycled T entering the plasma. If (4) is modified so that:

$$\dot{M}_{burn} = p_{burn}(\eta_{pellet}\dot{M}_{inject} + \eta_{recycled}\dot{M}_{wall}R) \tag{9}$$

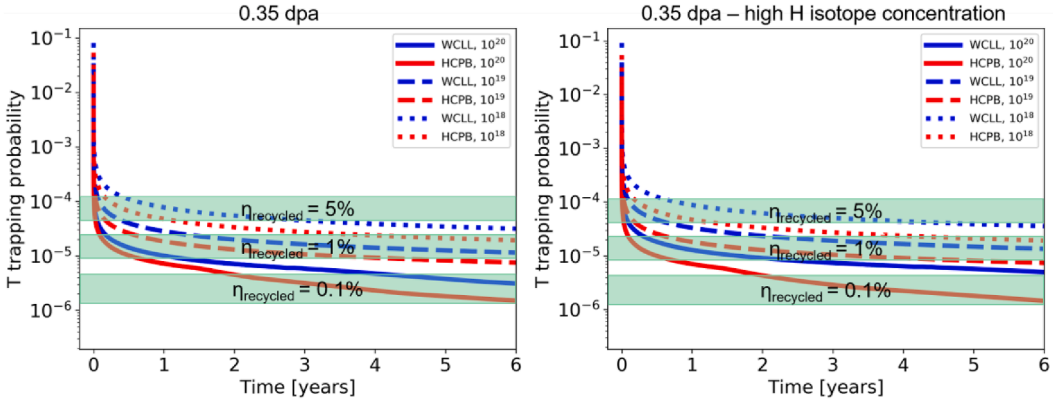

Fig. 8. T trapping probability as a function of time, in fpy, in the "high dpa" damaging scenarios with (right) and without (left) simultaneous hydrogen isotope loading, assuming a 0.8 mm W cladding. The upper limits for T trapping given by eq. (8) are shown shaded in green for $\eta_{recycled}$ values of 5%, 1% and 0.1%. (For interpretation of the references to color in this figure legend, the reader is referred to the web version of this article.)

with $\eta_{recycled}$ representing a fueling efficiency of T recycled from the wall, then the inequation governing $p_{trapped}$ changes to:

$$p_{trapped} \ll (TBR-1)\frac{p_{burn}\left(\eta_{pellet} - R\left(\eta_{pellet} - \eta_{recycled}\right)\right)}{1 - p_{burn}\eta_{pellet}} \quad (10)$$

Since $p_{trapped}$ varies in time as the traps are saturated and the net diffusion flux into the wall drops due to the flattening of the profile, it makes sense to repeat the above for the total amounts of trapped $N_{Trapped}$ and excess produced Tritium N_{Excess}:

$$N_{Excess} = (TBR-1)\dot{M}_{Burn}\Delta t$$

$$N_{Trapped} = \dot{M}_{wall}\int p_{trapped}$$

To reach T-self-sufficiency the total numbers have to satisfy $N_{Trapped} \ll N_{Excess}$. This finally leads to the result:

$$\langle p_{trapped}\rangle = \frac{\int p_{trapped}}{\Delta t} = \frac{\int \dot{M}_{trapped}}{\dot{M}_{wall}\Delta t} \ll (TBR-1)\frac{p_{burn}\left(\eta_{pellet} - R\left(\eta_{pellet} - \eta_{recycled}\right)\right)}{1 - p_{burn}\eta_{pellet}}$$

The right hand side is the same result as in eq. (10) but the left hand side can be easily extracted from the trapped amount calculated by TESSIM-X.

In Fig. 8, the averaged T trapping probabilities for the 0.35 dpa damaging scenarios with and without simultaneous H isotope loading are shown for a 0.8 mm W-clad wall as a function of time, assuming 50% of the impinging flux is T. Initially, the trapping probability is high because all traps are empty, so T atoms penetrating the wall are likely to be trapped. As the traps are filled, it becomes progressively unlikelier for T to be trapped, because impinging T must diffuse deeper into the bulk to encounter empty traps. Naturally, if the flux of T is lower, this decrease in the trapping probability happens more slowly. Shaded in green are the approximate upper limits for the T trapping probability, calculated with eq. (10), for values of $\eta_{recycled}$ of 0.1%, 1% and 5%. As in [38], *TBR* was taken as 1.05 and p_{burn} was varied between 0.02 and 0.05. The value of R was set to 99.9%, and η_{pellet} was varied between 0.3 and 0.8. According to this simplified model, if $\eta_{recycled}$ is approximately 0.1%, trapping of T in the walls could compromise T self-sufficiency, regardless of the impinging particle flux, because the calculated trapping probability exceeds the limit imposed by eq. (10) even after 6 full-power years. If $\eta_{recycled}$ is roughly 1%, T trapping might only be an issue in areas where the impinging flux density is lower than 10^{20} D/T $m^{-2}s^{-1}$. If $\eta_{recycled}$ is around 5%, T trapping could potentially only be an issue if an impinging flux of 10^{18} D/T $m^{-2}s^{-1}$ is assumed. It must still be noted that, depending on the assumed value of $\eta_{recycled}$, it may take several years before the trapping probability fulfils the limit imposed by eq. (10). During this time, overall T losses will not be compensated by the excess T produced by breeding.

6. Conclusions

In this work, a code comparison between the well-established TMAP7 code and the TESSIM-X code was performed, showing good agreement for a DEMO-like simplified scenario. Due to inherent limitations of TMAP7, TESSIM-X was then used to provide assessments of T permeation and retention for the DEMO WCLL and HCPB FW concepts under varying impinging particle fluxes, damage levels, and wall configurations. The results of these simulations are listed in Table 3 for the highest flux assumption (with 50% of the flux corresponding to T) and a damage level of 0.35 dpa. It was shown that substantial T losses due to retention may be expected in a W-containing wall, totaling several hundred grams of T sequestered at the end of life of the 2nd BB. T permeation may occur if the W cladding is sufficiently thin (0.8 mm), and could be in excess of 150 mg T per full-power day. If no W-containing cladding is used, permeation occurs in all cases due to gas loading, and could be in the range of several grams per day, while retention is reduced by roughly 1 order of magnitude relative to the W-containing cases.

The impact of retention on the T fuel cycle was assessed with the aid of a simplified model based on [38], which was extended to include fueling from recycled T. This model showed that, particularly if the fueling efficiency from recycled T or the impinging wall fluxes are low, T retention in the FW could pose an issue for T self-sufficiency.

While the results shown in this work may appear dire, it should be noted that they are based on several unverified assumptions. Regarding the input parameters, large uncertainties remain in the predicted DEMO wall fluxes and energies, due to uncertainties in the DEMO plasma scenario. To address this issue, the wall flux was varied in the simulations by two orders of magnitude, but improved predictions of the DEMO wall profile would be required to improve the accuracy of the simulations. Recent experimental and modeling results show that simultaneous loading with hydrogen isotopes during damaging leads to a higher concentration of traps in W [24]. This effect has been included in the modeling work shown here, but has not been experimentally verified at DEMO-relevant temperatures. For this reason, two damaging scenarios were included in the simulations at the highest damage levels, with and without H isotope loading. As the diffusion behavior of T through functionally graded W/EUROFER interlayers is presently unknown, wall configurations were included in the models which assumed that the full FGM system behaved like W or like EUROFER. While the actual behavior of the FGM system will likely lie somewhere in between these extremes, this approach is intended to provide upper and lower bounds for T permeation and retention. As the behavior of the W/EUROFER interface is also unknown, interface traps or barriers have not been included in the model, and it has been assumed that the T flux is conserved (no sinks at the interface) and there is equilibrium in the chemical potential at both sides of the interface. With regard to the surface properties, the W cladding has been modeled with the properties of solid W [39]. However, experimental data from literature indicates that plasma-sprayed W, as is proposed for DEMO [30], may lead to lower permeation rates than e.g. magnetron-sputtered W on steel, likely due to open porosity [40]. Also in the event of a EUROFER-only wall, the formation of a rough surface morphology and W and Ta surface enrichment [33,34] could potentially influence T uptake. Lastly, the surface boundary conditions at the inlet and outlet side can in principle play a role on the permeation behavior. To study this, the choice of a surface-limited boundary condition instead of a diffusion-limited boundary condition as was used in this work is discussed in Section 4. It was determined that applying a surface-limited boundary condition at the inlet side could lead to a slightly increased steady-state permeation flux. However, this effect is relatively small (10% increase), and is considered to lie within the uncertainties of the other input parameters.

Nevertheless, the assumptions used in this work are designed to provide a conservative (i.e., pessimistic) preliminary estimate of T permeation and retention in DEMO, and are therefore aimed at helping to guide future design and experimental work. With this information, upcoming efforts can be aimed at tackling these uncertainties, thereby contributing to the improvement of future modeling work.

CRediT authorship contribution statement

R. Arredondo: Conceptualization, Methodology, Software, Validation, Formal analysis, Writing - original draft, Visualization. **K. Schmid:** Conceptualization, Methodology, Software, Formal analysis. **F. Subba:** Software, Formal analysis, Resources. **G.A. Spagnuolo:** Conceptualization, Resources, Project administration.

Declaration of Competing Interest

The authors declare that they have no known competing financial interests or personal relationships that could have appeared to influence the work reported in this paper.

Acknowledgements

The authors would like to thank Dr. Schwarz-Selinger for his helpful and insightful comments.

This work has been carried out within the framework of the EUROfusion Consortium and has received funding from the Euratom research and training programme 2014-2018 and 2019-2020 under grant agreement No 633053. The views and opinions expressed herein do not necessarily reflect those of the European Commission.

References

[1] A.J. Donné, J. Fusion Energ. 38 (2019) 503–505.
[2] G. Federici, C. Skinner, J. Brooks, J. Coad, C. Grisolia, A. Haasz, A. Hassanein, et al., Nucl. Fusion 41 (2001) 1967–2137.
[3] H.A. Boniface, N.V. Gnanapragasam, D.K. Ryland, S. Suppiah, A. Perevezentsev, Fusion Sci. Technol. 71 (2017) 241–245.
[4] F. Cismondi, G.A. Spagnuolo, L.V. Boccaccini, P. Chiovaro, S. Ciattaglia, I. Cristescu, C. Day, et al., Fusion Eng. Des. 157 (2020) 111640.
[5] K. Katayama, Y. Someya, K. Tobita, H. Nakamura, H. Tanigawa, M. Nakamura, N. Asakura, et al., Fusion Sci. Technol. 71 (2017) 261–267.
[6] K. Schmid, Phys. Scr. T167 (2016) 14025.
[7] K. Schmid, U. von Toussaint, T. Schwarz-Selinger, J. Appl. Phys. 116 (2014) 134901.
[8] K. Schmid, V. Rieger, A. Manhard, J. Nucl. Mater. 426 (2012) 247–253.
[9] G.R. Longhurst, TMAP7 User Manual (2008).
[10] G. de Temmerman, M.J. Baldwin, D. Anthoine, K. Heinola, A. Jan, I. Jepu, J. Likonen, et al., Nucl. Mater. Energ. 12 (2017) 267–272.
[11] M. Shimada, C.N. Taylor, Nucl. Mater. Energ. 19 (2019) 273–278.
[12] E. Martelli, A. Del Nevo, P. Arena, G. Bongiovì, G. Caruso, P.A. Di Maio, M. Eboli, et al., Int. J. Energy Res. 42 (2018) 27–52.
[13] F. Hernández, P. Pereslavtsev, Q. Kang, P. Norajitra, B. Kiss, G. Nádasi, O. Bitz, Fusion Eng. Des. 124 (2017) 882–886.
[14] G. Holzner, Determining fundamental transport parameters of hydrogen isotopes in tungsten, Dissertation, München (2020).
[15] A. Aiello, I. Ricapito, G. Benamati, R. Valentini, Fusion Sci. Technol. 41 (2002) 872–876.
[16] G.A. Esteban, A. Peña, I. Urra, F. Legarda, B. Riccardi, J. Nucl. Mater. 367–370 (2007) 473–477.
[17] Y. Xu, Z.-S. Wu, L.-M. Luo, X. Zan, X.-Y. Zhu, Q. Xu, Y.-C. Wu, Fusion Eng. Des. 155 (2020) 111563.
[18] A. Mutzke, R. Schneider, W. Eckstein, R. Dohmen, K. Schmid, U. von Toussaint, G. Badelow, SDTrimSP Version 6.00, Max-Planck-Institut für Plasmaphysik (2019).
[19] W. Eckstein, Computer Simulation of Ion-Solid Interactions, Springer, Berlin Heidelberg, Berlin, Heidelberg, 1991.
[20] R. Behrisch, G. Federici, A. Kukushkin, D. Reiter, J. Nucl. Mater. 313–316 (2003) 388–392.
[21] R.A. Anderl, D.F. Holland, G.R. Longhurst, R.J. Pawelko, C.L. Trybus, C.H. Sellers, Fusion Technol. 21 (1992) 745–752.
[22] G. Federici, W. Biel, M.R. Gilbert, R. Kemp, N. Taylor, R. Wenninger, Nucl. Fusion 57 (2017) 92002.
[23] O.V. Ogorodnikova, Z. Zhou, K. Sugiyama, M. Balden, G. Pintsuk, Y. Gasparyan, V. Efimov, Nucl. Fusion 57 (2017) 36011.
[24] M. Pečovnik, E.A. Hodille, T. Schwarz-Selinger, C. Grisolia, S. Markelj, Nucl. Fusion 60 (2020) 36024.
[25] S. Wiesen, D. Reiter, V. Kotov, M. Baelmans, W. Dekeyser, A.S. Kukushkin, S. W. Lisgo, et al., J. Nucl. Mater. 463 (2015) 480–484.
[26] M. Iwamoto, Y. Fukai, Mater. Trans., JIM 40 (1999) 606–611.
[27] F. Besenbacher, S.M. Myers, P. Nordlander, J.K. No, rskov, J. Appl. Phys. 61 (1987) 1788–1794.
[28] T. Tanabe, Y. Furuyama, S. Imoto, J. Nucl. Mater. 145–147 (1987) 305–308.
[29] G. Mazzini, T. Kaliatka, M.T. Porfiri, Fusion Eng. Des. 146 (2019) 510–513.
[30] T. Emmerich, D. Qu, R. Vaßen, J. Aktaa, Fusion Eng. Des. 128 (2018) 58–67.
[31] D.D. Qu, W.W. Basuki, J. Aktaa, Fusion Eng. Des. 98–99 (2015) 1389–1393.
[32] D.D. Qu, W.W. Basuki, J. Gibmeier, R. Vaßen, J. Aktaa, Fusion Sci. Technol. 68 (2015) 578–581.
[33] K. Sugiyama, M. Balden, S. Elgeti, T. Höschen, M. Oberkofler, J. Roth, W. Jacob, Nucl. Mater. Energ. 16 (2018) 114–122.
[34] R. Arredondo, M. Balden, A. Mutzke, U. von Toussaint, S. Elgeti, T. Höschen, K. Schlueter, et al., Nucl. Mater. Energ. 23 (2020) 100749.
[35] K. Schmid, M. Zibrov, Nucl. Fusion (2021).
[36] M.A. Pick, K. Sonnenberg, J. Nucl. Mater. 131 (1985) 208–220.
[37] F. Tavassoli, Procedia Eng. 55 (2013) 300–308.
[38] R.P. Doerner, G.R. Tynan, K. Schmid, Nucl. Mater. Energ. 18 (2019) 56–61.
[39] G. Holzner, T. Schwarz-Selinger, T. Dürbeck, U. von Toussaint, Phys. Scr. T171 (2020) 14034.
[40] R.A. Anderl, R.J. Pawelko, M.R. Hankins, G.R. Longhurst, R.A. Neiser, J. Nucl. Mater. 212–215 (1994) 1416–1420.